LAWRENCE
LIVERMORE
NATIONAL
LABORATORY

LLNL-TR-671402

Hydrothermal Alteration of Glass from Underground Nuclear Tests: Formation and Transport of Pu-clay Colloids at the Nevada National Security Site

M. Zavarin, P. Zhao, C. Joseph, J. Begg, M. Boggs, Z. Dai, A. B. Kersting

May 27, 2015

Disclaimer

This work performed under the auspices of the U.S. Department of Energy by Lawrence Livermore National Laboratory under Contract DE-AC52-07NA27344.

Hydrothermal Alteration of Glass from Underground Nuclear Tests: Implications for Colloid Formation and Plutonium Transport at the Nevada National Security Site

M. Zavarin*, P. Zhao, C. Joseph, J. Begg, M.A. Boggs, Z. Dai, and A.B. Kersting

Glenn T. Seaborg Institute, Physical & Life Sciences, L-231, Lawrence Livermore National Laboratory,

Livermore, CA 94550

*Corresponding Author: zavarin1@llnl.gov

Introduction

The testing of nuclear weapons at the Nevada National Security Site (NNSS), formerly the Nevada Test Site (NTS), has led to the deposition of substantial quantities of plutonium into the environment. Approximately 2.8 metric tons (3.1×10^4 TBq) of Pu were deposited in the NNSS subsurface as a result of underground nuclear testing (Smith et al., 2003). While ^{3}H is the most abundant anthropogenic radionuclide deposited in the NNSS subsurface (4.7×10^6 TBq), plutonium is the most abundant from a molar standpoint. The only radioactive elements in greater molar abundance are the naturally occurring K, Th, and U isotopes. ^{239}Pu and ^{240}Pu represent the majority of alpha-emitting Pu isotopes.

The extreme temperatures associated with underground nuclear tests and the refractory nature of Pu results in most of the Pu (98%) being sequestered in melted rock, referred to as nuclear melt glass (Iaea, 1998). As a result, Pu release to groundwater is controlled, in large part, by the leaching (or dissolution) of nuclear melt glass over time.

The factors affecting glass dissolution rates have been studied extensively. Rates of glass dissolution are dependent on pH, silica content, and temperature (Mazer, 1987), as well as

surface area and other factors. The temperature dependence of glass dissolution rates is exponential (Declercq et al., 2013). As a result, high temperatures may substantially exacerbate the rate of Pu release.

Underground nuclear test-related thermal effects may exist for 25 years or more (Carle et al., 2003). The temperature history will depend on the size of the underground nuclear test and its depth of burial, the permeability of the surrounding rock, and the groundwater velocities through the melt glass zone. At the Cheshire site (200-500 kt test, 1167 m depth of burial, 542 m below water table), groundwater was predicted to re-saturate the melt glass 20 days after the detonation. At that time, the melt glass temperature was predicted to be 160ºC. By 700 days, the melt glass temperature was predicted to drop to 90ºC. At the Greeley site (870 kt test, 1217 m depth of burial, 602 m below water table), groundwater was predicted to re-saturate the melt glass 60 days after the detonation. At that time, the melt glass temperature was predicted to be 200 ºC and decreased to 125ºC by 700 days. At the Almendro site (200-1000 kt test, 1064 m depth of burial, 378 m below water table), the shallower water table and low permeability of the surrounding rock leads to much slower re-saturation of the melt glass; the melt glass zone was predicted to fully re-saturate only after 7 years. At that point, the maximum melt glass temperature was measured to be 215ºC and was 160ºC 23 years later. At smaller underground nuclear tests such as Cambric (0.75 kt-test, 294 m depth of burial, 74 m below water table), hydrothermal effects are predicted to be much smaller, with temperatures dropping below 40ºC in just a few years (Carle et al., 2006).

The composition of melt glass at the NNSS is closely related to the composition of the host rock in which the test was detonated. The majority of tests were detonated in rhyolitic rock. At a result, melt glass is dominated by silica (~75 wt.%) and Al_2O_3 (~15 wt.%). The radiologic

component represents a very small mass fraction of melt glass. Based on the total Pu inventory (2.8 Mg) and an estimated mass of melt glass produced as a result of underground nuclear testing (maximum yields as reported in (Doe, 2000) and a melt glass formation estimate of 700 Mg glass per kt yield), we arrive at an average Pu concentration of 60 ppb in melt glass (160 Bq/g $^{239+240}$Pu). Dissolution of rhyolitic glasses will typically lead to the formation of clay and zeolite secondary minerals. The trace levels of radionuclides contained in the melt glass are unlikely to have a significant impact on glass dissolution rates.

The dissolution of Pu-containing borosilicate nuclear waste glasses at 90ºC has been shown to lead to the formation of dioctahedral smectite colloids (Buck and Bates, 1999). Due to its high affinity for mineral surfaces, plutonium was found to associate with the colloidal fraction in solution. Indeed, the potential formation and transport of Pu-bearing colloids as a result of nuclear waste glass dissolution was reported over 20 years ago (Bates et al., 1992). While the clay colloids are dominated by smectite, Bates et al. (1992) suggested that Pu may be predominantly associated with the phosphate mineral brockite. However, the types of colloids produced and the nature of the Pu-association with colloids will likely depend on the glass composition, water chemistry, and reaction temperatures.

Colloid facilitated transport of Pu at the NNSS has been observed. In 1999, Kersting et al. (1999) identified Pu concentrations as high as 0.03 Bq/L 1.3 km down-gradient from the Benham test and determined that the migration was facilitated by colloids. The colloids were composed of clays (illite and smectite), zeolites (mordenite and clinoptilolite/heulandite), and cristobalite. The mineralogy of the colloids was consistent with the alteration of rhyolitic tuffs at the NNSS and a common mineralogy observed at the NNSS. However, it was also suggested that smectite is a common product of the alteration of high level waste glass. Thus, the mineral colloids Kersting

et al. (1999) observed 1.3 km from the Benham test site may have come from natural or anthropogenic sources.

Recent groundwater samples collected from a number of contaminated wells have yielded a wide range of Pu concentrations from 0.00022 to 2.0 Bq/L (Zhao et al., 2014). While Pu concentrations tend to fall below the Maximum Contaminant Level (MCL) established by the Environmental Protection Agency (EPA) for drinking water (0.56 Bq/L), we do not yet understand what factors limit the Pu concentration or its transport behavior. To quantify the upper limit of Pu concentrations produced as a result of melt glass dissolution and determine the nature of colloids and Pu associations, we performed a 3 year nuclear melt glass dissolution experiment across a range of temperatures (25-200 °C) that represent hydrothermal conditions representative of the underground nuclear test cavities (when groundwater has re-saturated the nuclear melt glass and glass dissolution occurs). Colloid loads and Pu concentrations were monitored along with the mineralogy of both the colloids and the secondary mineral phases. The intent was to establish an upper limit for Pu concentrations at the NNSS, provide context regarding the Pu concentrations observed at the NNSS to date and the Pu concentrations that may be observed in the future. The results provide a conceptual model for the risks posed by Pu migration at the NNSS.

Materials and Methods

Glass preparation

Nuclear melt glass was retrieved from underground nuclear test debris samples available at LLNL. Four melt glass samples were selected due to their uniform appearance as solid black glass fragments with little if any apparent secondary minerals present. The four samples were combined and yielded a total of about 10 g of melt glass. The glass was crushed using mortar and

pestle (in water to minimize dispersion of radioactivity) and wet sieved through a 90 μm-sieve. At the conclusion of wet sieving, a total of about 200 mL of solution containing melt glass was produced. To establish a lower limit particle size in our stock glass, we used a 10 minute settling cutoff (repeated three times in >18 MΩ·cm water) in which the supernatant containing clay-sized melt glass particles was discarded. This produced a melt glass stock with a lower limit particle diameter of ~15 μm.

HF was used to clean the melt glass and remove any secondary minerals from the surface of the glass fragments. This was accomplished by exposing the glass to a 1% HF solution for 1 min. At the end of the HF reaction, the 10 minute settling time cutoff was repeated 3 times. This produced a clean stock melt glass with a particle size range of 15-90 μm. Upon completion of the cleaning and size separation, the melt glass was dried.

The stock melt glass was characterized by Scanning Electron Microscopy (JEOL JSM-7401F SEM), Transmission Electron Microscopy (Philips CM 300 FEG TEM operating at 300kV and equipped with a Gatan Imaging Filter (GIF) with a 2k × 2k CCD camera and an EDX detector), gamma counting (high-purity germanium detectors, Ortec, Ortec's Maestro data acquisition software combined with gamma-ray spectrum analysis using LLNL-developed software package (GAMANAL), and total Pu analysis by Multiple Collector–Inductively Coupled Plasma–Mass Spectrometry (Nu Plasma MC-ICP-MS, Nu Instruments). SEM images indicated a homogeneous glass morphology and no additional secondary phases (Figure 1). A focused ion beam was used to prepare a TEM sample and revealed small magnetite inclusions (Figure 2). The magnetite nanoparticles were the only crystalline phase observed in the melt glass and were present at trace levels. Gamma counting combined with MC–ICP–MS identified the radiologic components of the glass as ^{137}Cs (2155±17 Bq/g), ^{60}Co (96.3±3.7 Bq/g), ^{152}Eu

(37.9±1.5 Bq/g), and $^{239+240}$Pu (46.6 Bq/g). All radiologic measurements were decay corrected to September 23, 1992, the date of the last underground nuclear test conducted at the NNSS (Smith et al., 2003).

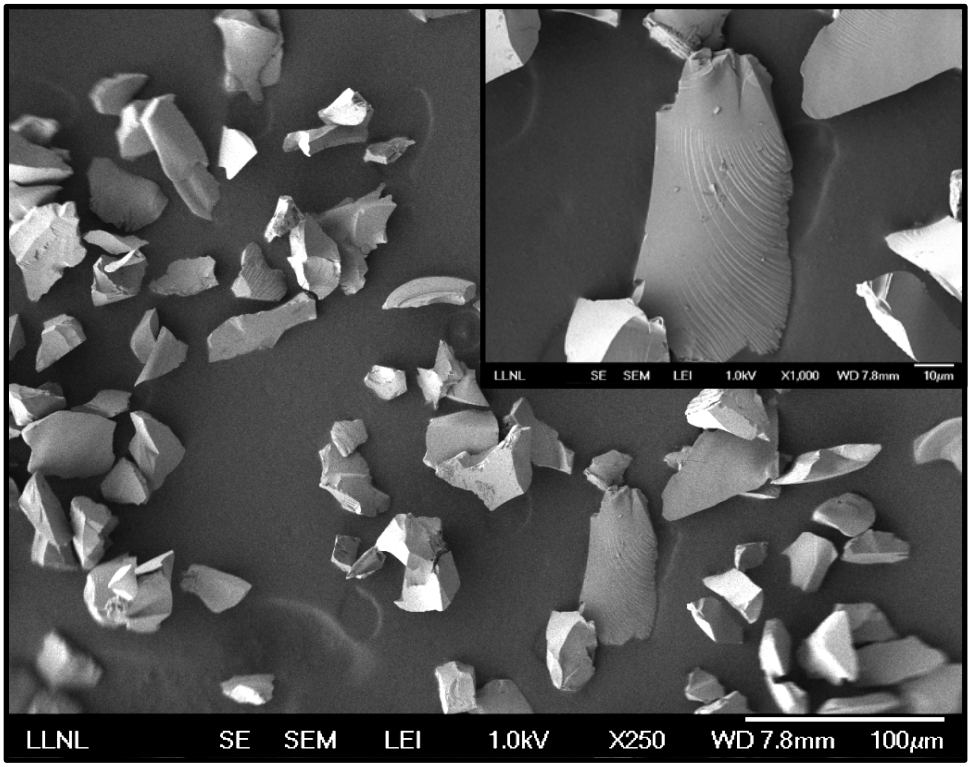

Figure 1. Crushed, sieved, and HF-treated nuclear melt glass used in hydrothermal experiments.

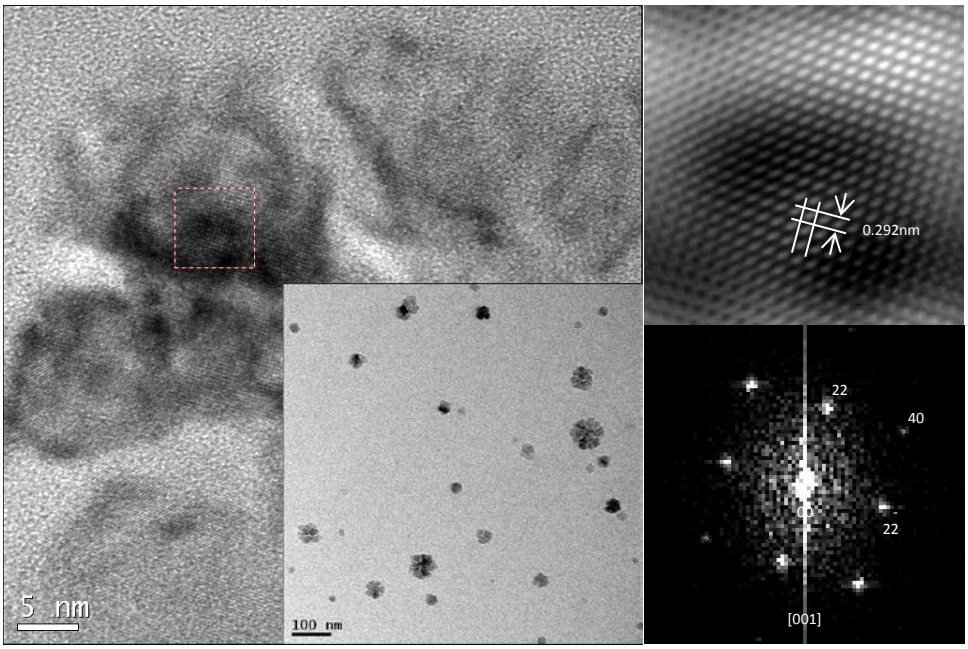

Figure 2. TEM image of melt glass reveals magnetite (Fe_3O_4) nanoparticles embedded in a glass matrix. Analysis with an energy dispersive X-ray detector (EDX) did not indicate accumulation of Pu in the magnetite phase.

Hydrothermal Experiments

All solutions were prepared using ultrapure water (Milli-Q Gradient System, > 18 MΩ·cm) and, apart from the Pu stock solution, ACS grade chemicals without further purification. For the glass alteration experiments, four samples, each containing 2 g of melt glass in 500 mL of a 5 mM NaCl/0.7 mM $NaHCO_3$ solution (pH 8) were prepared (solution composition based on a simplified low ionic strength sodium bicarbonate water present at the NNSS). Samples were stored at four temperatures: room temperature (~ 25°C), 80°C, 140°C, and 200°C. The room temperature sample was stored in a Teflon container. The higher temperature samples were placed in 600 mL Parr pressure vessels (Model 4764 in Titanium Grade 2, with polytetrafluoroethylene (PTFE) flat gasket closure and 1000 psi gold-faced rupture disk with titanium orifice cone). The titanium was passivated using boiling 8 M HNO_3 which was

followed by a Milli-Q water rinse and heating to 400°C overnight. Parr bombs were leak tested for 4 days prior to the start of the experiments. No mass loss was found.

Samples were collected at three time points over a 3 year period (457, 644, and 994 days). At each sampling time, containers were cooled to room temperature overnight. The cooled samples were then shaken by hand and a ten minute settling time was used to remove original glass material from the supernatant. Approximately 400 mL of supernatant and a small amount of solid material was removed for analysis. Solutions in Parr bombs were replenished with fresh 5 mM NaCl/0.7 mM $NaHCO_3$ solution (pH 8) to a total volume of 500 mL and placed back in their respective ovens. Due to the sampling procedure, the glass experienced alteration over the entire 3 year period. However, the solution phase evolution was likely affected by the sampling at intermediate stages of the experiment.

Sample Characterization

At each time point, the supernatant was initially gamma counted to determine the total concentration of gamma emitting radionuclides. A portion of the sample was then taken for total Pu analysis (by MC–ICP–MS). The remaining sample was vacuum filtered through a 20 nm Whatman Anodisc47 membrane filter. The filter was washed with several milliliters of Milli-Q water and dried to determine the >20 nm colloid mass fraction. The colloid mineralogical composition was determined by re-suspending the >20 nm colloids in Milli-Q water and depositing the solids on planchets or Cu grids followed by XRD/SEM/TEM characterization. Characterization of the >20 nm colloidal material by XRD was performed using a Bruker D8 X-ray diffractometer using radiation from a copper target tube (Cu K_α) and operating at 40 kV, 40 mA, and a scanning speed of 0.5°/min.

The radiologic composition of the <20 nm fraction was analyzed by MC–ICP–MS (for Pu) and gamma counting. The <20 nm filtrate does not represent the truly aqueous fraction as colloid in the 2-20 nm range may be present in the filtrate. Nevertheless, the difference in the radiologic composition of the original supernatant and the filtrate represent a lower limit to the fraction of radionuclides associated with colloids.

Pu Desorption Experiments

Pu desorption behavior from colloids produced by the hydrothermal alteration of nuclear melt glass was compared to experiments in which Pu was adsorbed to montmorillonite colloids. For the latter experiments, a ^{238}Pu (98.9 % ^{238}Pu, 0.11 % ^{241}Pu, and 0.1 % ^{239}Pu by activity) spike was used. Impurities were removed from the spike by loading Pu onto a Bio Rad AG 1-8X resin, in 8 M HNO_3, and eluting as Pu(III) with a HI:HCl mixture. The eluent was heated to dryness several times to remove excess HI and subsequently dissolved in 1.0 M HCl. The oxidation state of the Pu spike solution was verified by LaF_3 precipitation (Kobashi et al., 1988) to be IV (99 %). ^{238}Pu concentrations were determine by Liquid Scintillation Counting (Packard Tri-Carb TR2900 LSA).

Preparation of a SWy-1 montmorillonite colloid stock solution (Source Clays Repository of the Clay Minerals Society) used in this study is described in Zavarin et al. (2012). Briefly, montmorillonite was treated with 1 mM HCl and 30 mM H_2O_2 to remove salts and limit redox active species. The clay was homoionized with 10 mM NaCl and dialized in >18 MΩ·cm water. After homoionization, the clay was suspended in >18 MΩ·cm water and centrifuged at 180 *g* for 5 min to sediment particles >2 μm. The remaining supernatant was then centrifuged at 2500 *g* for 6 h to sediment all particles <50 nm. The suspension was dried at 40°C and solutions of 10 g/L montmorillonite were prepared in NaCl/$NaHCO_3$.

For the Pu-montmorillonite adsorption experiment, the ^{238}Pu(IV) spike was added to a solution of 0.1 g/L montmorillonite in 0.01 M NaCl to achieve 10^{-10} M Pu and the pH adjusted to 6.3 with NaOH. The solution was equilibrated under gentle agitation at 22°C for 16 months prior to use in desorption experiments. Oxidation state analysis by LaF_3 precipitation indicated that the Pu remained in the IV oxidation state throughout the equilibration period.

Pu desorption was performed on both the ^{238}Pu-montmorillonite suspension and the colloids produced in the hydrothermal experiments. In both cases, aliquots of the suspensions (^{238}Pu-montmorillonite: 5 mL; hydrothermally altered melt glass colloids: 10-40 mL depending on colloid load) were centrifuged at 10,000 rpm for 2 or 15 h. The supernatants were analyzed for their Pu concentration by LSC (^{238}Pu-montmorillonite) or MC–ICP–MS (hydrothermally altered melt glass colloids). The remaining solids were re-suspended in 10 mL (^{238}Pu-montmorillonite) or 1 mL (hydrothermally altered melt glass colloids) 0.008 M ethylenediaminetetraacetic acid (EDTA)/0.01 M NaCl solution. For the ^{238}Pu-montmorillonite samples, the total Pu concentration in the EDTA suspension was analyzed by LSC. The total $^{239+240}$Pu-load on the hydrothermally altered melt glass colloids was determined previously (see Sample Characterization). The EDTA suspensions were equilibrated for 4 days. After this time, the aqueous Pu concentration was determined in the supernatants. Based on these analyses, the percent Pu that is easily desorbed from colloids by EDTA was determined.

Results and Discussion

Hydrothermal alteration of melt glass

The strong temperature dependence of melt glass dissolution is evident from the SEM characterization of nuclear melt glasses over time (Figure 3). At room temperature, no evidence

of melt glass alteration can be observed at 994 days (Figure 4). However, the degree of glass alteration and formation of secondary phases increases with both time and temperature. The presence of secondary phases is not evident at 80°C but is prominent at both 140 and 200°C. The presence of the nuclear melt glass is evident in all samples except the 200°C 994 day sample. At 200°C, it appears that the original melt glass was completely altered by 994 days. Furthermore, while the alteration phases in all other samples appear to be dominated by smectite clay mineralogy, additional secondary phases appear at 200°C (Figure 3).

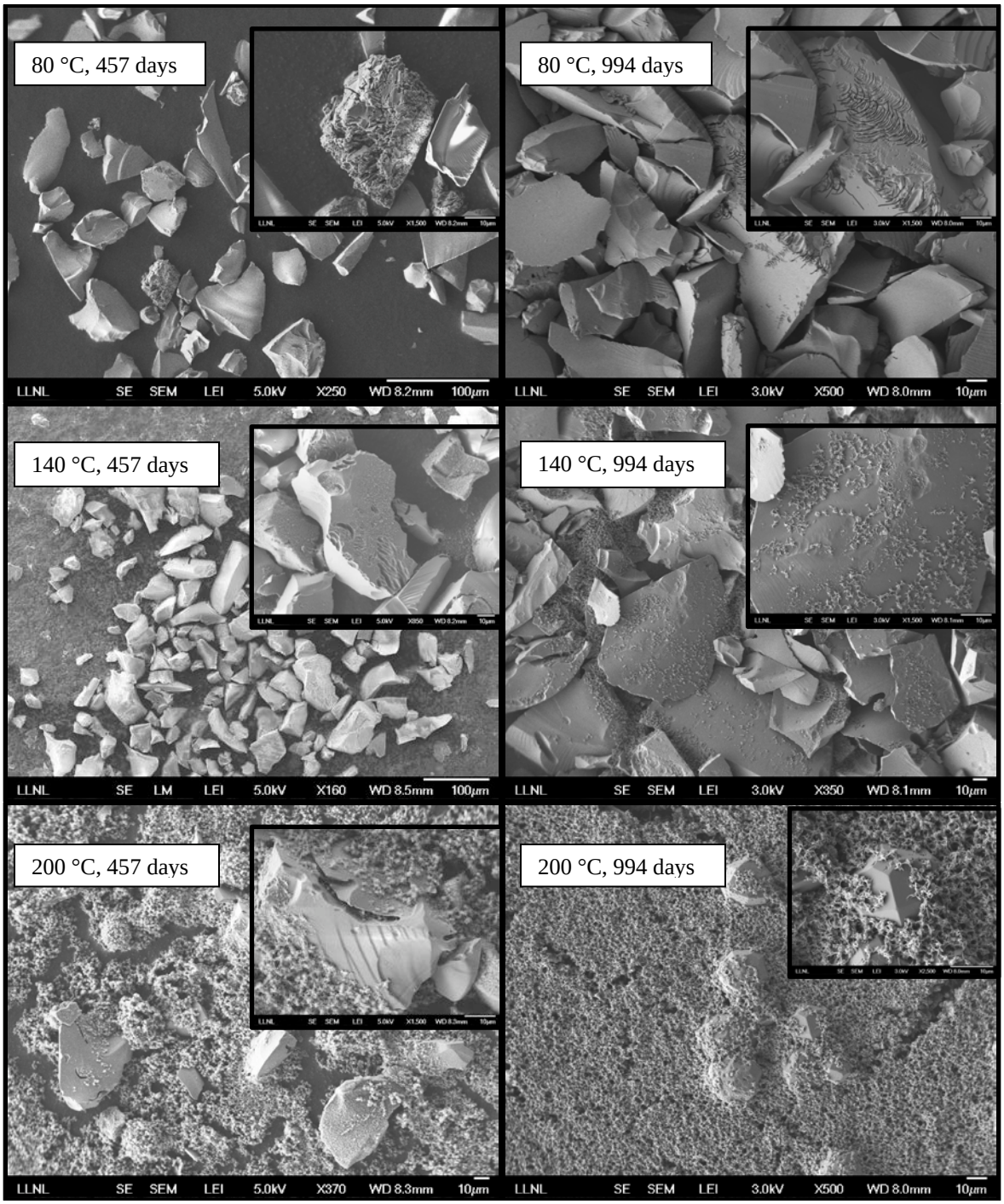

Figure 3. Morphology of hydrothermally altered melt glass (80, 140, and 200°C) after 457 and 994 days of reaction. At 80°C, the only visible evidence of glass dissolution are the etch pits located on the nuclear melt glass. At 140°C, both etch pits and the presence of a secondary phase (smectite) is evident. At 200°C, the original nuclear melt glass is absent by 994 days and is substituted by smectite clay combined with large crystalline zeolite phases.

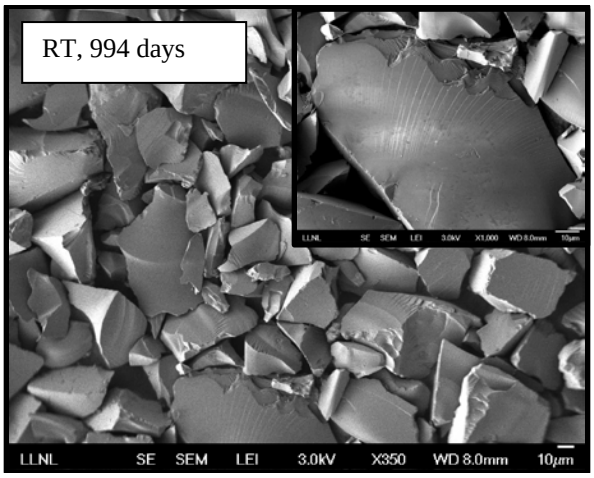

Figure 4. Morphology of melt glass after 994 days reaction at room temperature.

The mineralogical composition of the altered melt glass samples at the end of the experiment was determined qualitatively by XRD. Samples were deposited on zero-background plates fitted with domed covers to prevent dispersion of radioactive materials. The domed covers result in several broad peaks in the diffractograms (Figure 5). After background correction, the diffractograms suggest that formation of secondary phases at room temperature and 80°C was not significant over these timescales. However, a number of peaks are visible in the 140 and 200°C samples. At 140°C, the secondary minerals are dominated by smectite phases. At 200°C, we observe the formation of clinoptilolite and analcime zeolites in addition to smectite. The result is consistent with our SEM observations and the expected stabilization of zeolites at higher temperatures. It is also consistent with mineralogic characterization of colloids present in NNSS groundwater (Kersting et al., 1999).

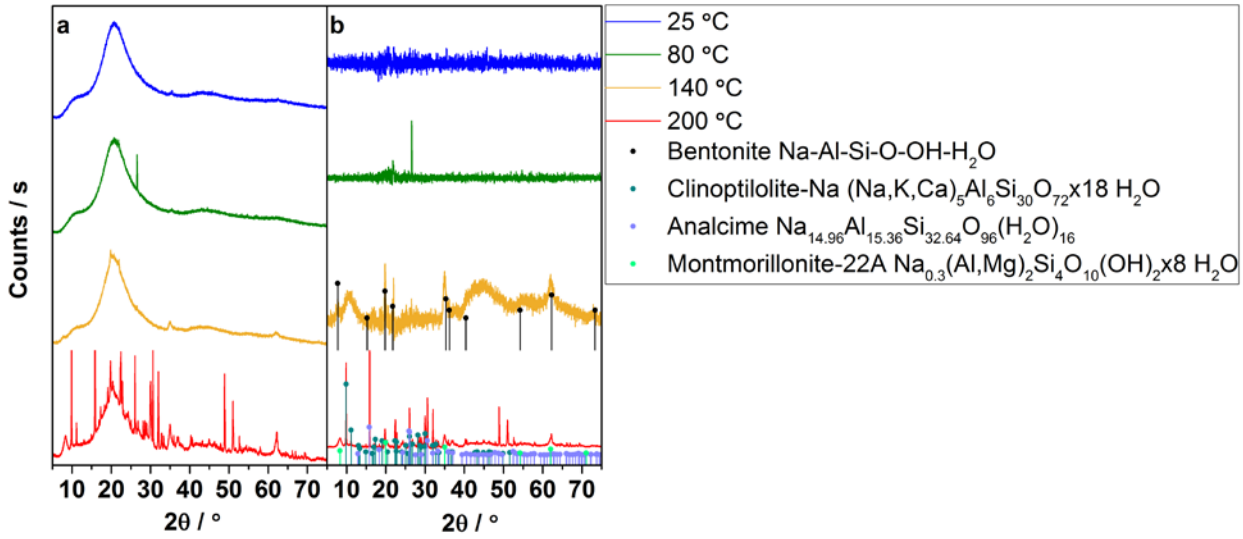

Figure 5. XRD of melt glass samples hydrothermally altered at 25, 80, 140, and 200°C for 994 days. (a) Raw data; (b) background-corrected diffractograms.

Formation of colloids and radionuclide release

Solution colloid loads, retained by the >20 nm pore size filters, suggest that hydrothermal alteration of melt glasses can yield high colloid loads in solution (Table 1). Colloid loads are highest in the 140 and 200°C samples in which substantial formation of secondary phases could be observed by SEM. In these samples, the colloid loads vary from 0.06 to 0.26 g/L. The variations likely represent measurement uncertainties that resulted from differences in settling time prior to supernatant removal as well as experimental errors (e.g., filtration membrane rupture). Solution major ion composition was determined at each sampling interval; no major changes in the Na/HCO_3/Cl background electrolyte composition were observed. Thus, differences in colloid load cannot be attributed to changes in solution composition (e.g. (Degueldre et al., 2000)). In the high temperature samples, colloid load is probably not limited

by the quantity of clay in the sample, but rather by coagulations/aggregation behavior of these clays under these conditions.

Small but measureable colloid concentrations were found in the 80°C samples. However, the nature of those colloids could not be determined from XRD or SEM. The colloid concentration in room temperature samples was below our detection limit (~ 0.005 g/L).

Table 1. Colloid load in solution as a function of temperature and time.

Time	Colloid load, g/L			
	25°C	80°C	140°C	200°C
457 days	0.000	0.011	0.239	0.070
644 days	0.002*	0.013	0.259	0.150
994 days	0.000	0.003*	0.073	0.062*

* Filtration membrane rupture noted during experiment. This leads to a lower apparent colloid load.

It is useful to compare the colloid loads observed in the hydrothermal alteration experiments to those observed in the field. A summary of recent measured colloid concentrations in NNSS water is provided in histogram form in Figure 6. Measured colloid concentrations vary from 1×10^{-6} to 1 g/L (5×10^{-4} g/L median value). The higher values likely do not represent ambient colloid concentrations in groundwater. Instead, the high values are likely an artifact of high groundwater pumping rates or incomplete well development which can lead to higher than expected colloid loads. Degueldre et al. suggested that colloid loads in deep low ionic strength groundwaters from crystalline rock will likely not exceed 0.0001 g/L under constant hydrogeochemical conditions and may only reach 0.01 g/L during transient hydrothermal or tectonic events (Degueldre et al., 1996a; Degueldre et al., 1996b). Colloid loads in higher ionic strength waters will tend toward even lower values (Degueldre et al., 1989). While the welded tuffs of Pahute Mesa are not representative of the granitic crystalline rocks examined by

Degueldre, the welded tuffs of Pahute Mesa can be categorized as deep low ionic strength groundwaters from crystalline rock. Furthermore, Degueldre examine the stability of colloids in J-13 waters and found that its groundwater composition leads to similar yet somewhat lower colloid loads when compared to very low ionic strength waters typical of granitic rock (Degueldre et al., 2000). Thus, we expect that colloid concentrations in groundwater transported downgradient from the nuclear test cavities will likely be lower than the concentrations found in the 140 and 200°C hydrothermal nuclear melt glass alteration experiments.

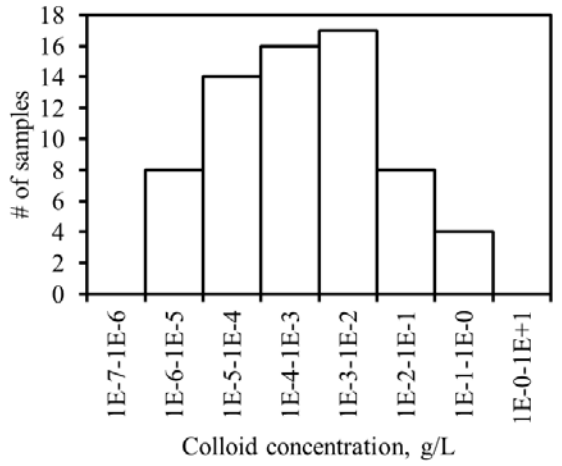

Figure 6. Recent observation of colloid concentrations in NNSS water (Navarro-Intera, 2014).

Hydrothermal alteration of the melt glass leads to the release of radionuclides into solution (Table 2). Temperature has a significant effect on Pu concentrations in solution at each time point. The average Pu concentration in the room temperature samples (0.03 Bq/L) was nearly two orders of magnitude lower than at 80°C (2 Bq/L) and nearly three orders of magnitude lower than at 140 and 200°C (13 and 15 Bq/L, respectively). A consistent increasing trend in Pu concentration was not observed with time. However, it should be noted that at each time point, approximately 80% of the fluid was removed from the reaction vessels and replaced with

radionuclide-free (and colloid-free) buffer solution. Thus, these measurements do not represent the evolution of fluids as a function of contact time. Furthermore, the three sampling times are insufficient to warrant a detailed discussion of the time-dependence of Pu release. The temperature dependent Pu concentrations suggest that the early-time hydrothermal (high T) conditions expected at underground nuclear tests can lead to high Pu fluxes to groundwater and that release rates under long-term ambient conditions will likely be substantially reduced.

Table 2. Radiologic composition of supernatant before colloid filtration.

Time	25 °C	80 °C	140 °C	200 °C
	---------- ^{60}Co, Bq/L ----------			
457 days	ND	4.6(0.6)	47.8(0.9)	42.1(1.3)
644 days	ND	ND	30.4(4.1)	104(7)
994 days	ND	3.0(0.4)	21.1(0.6)	25.3(0.7)
	---------- ^{137}Cs, Bq/L ----------			
457 days	8.7(0.3)	149(1)	1379(12)	1111(10)
644 days	15.7(0.4)	147(2)	870(9)	512(7)
994 days	5.3(0.2)	150(1)	952(9)	490(3)
	---------- ^{152}Eu, Bq/L ----------			
457 days	ND	2.4(0.5)	17.8(0.6)	13.5(0.9)
644 days	ND	ND	ND	31.4(2.8)
994 days	ND	2.0(0.3)	11.8(0.7)	9.8(0.6)
	---------- Pu, Bq/L ----------			
457 days	0.0271(0.0015)	1.63(0.08)	12.6(0.7)	11.6(0.7)
644 days	0.0574(0.0015)	2.01(0.04)	13.8(0.2)	29.6(0.5)
994 days	0.0153(0.0028)	2.15(0.44)	11.3(2.2)	4.6(0.9)

* ND=not detected. Measurement error in parentheses. EPA MCLs for ^{60}Co, ^{137}Cs, ^{152}Eu, and Pu are 3.7, 7.4, 7.4, and 0.55 Bq/L.

While the focus of this effort has been the examination of Pu release from melt glass, it is instructive to examine the release of gamma-emitting radionuclides. The trend in temperature dependence for ^{60}Co, ^{137}Cs, and ^{152}Eu release follows that of Pu. Thus, preferential leaching of these radionuclides is not observed. One exception is the ^{137}Cs/Pu ratio at room temperature which is more pronounced than at other temperatures and suggests some preferential leaching of ^{137}Cs relative to Pu.

The four radionuclides detected as a result of glass leaching have been observed in groundwater at the NNSS. Kersting et al. (1999) detected these same radionuclides 1.3 km down-gradient from the Benham test. While the source of Pu was identified isotopically as the Benham test, the source of ^{60}Co, ^{137}Cs, and ^{152}Eu could not be confirmed. Nevertheless, it is instructive to note that ratios of ^{60}Co, ^{137}Cs, and ^{152}Eu to Pu in our hydrothermal melt glass alteration experiments are equivalent, within an order of magnitude, to the ratios observed in the Kersting et al. (1999) data. While this does not provide direct evidence regarding the source of radionuclides at ER-20-5, it suggests that the radiologic composition of groundwater at ER-20-5 is compositionally similar to the radiologic composition of groundwater produced as a result of hydrothermal alteration of melt glass.

From the perspective of groundwater contamination, it is noteworthy that, in the room temperature experiments, the concentration of all four radionuclides is at or below the Maximum Contaminant Level (MCL) established for these radionuclides in drinking water by the US Environmental Protection Agency (EPA). The radionuclide concentrations fall at or above (for ^{60}Co and ^{152}Eu) and well above (for ^{137}Cs and Pu) the EPA limits in the 140°C and 200°C experiments. This implies that early time hydrothermal alteration of melt glass may have a significant effect on groundwater contamination. However, it must be remembered that the melt glass alteration experiments provide an upper limit of radiologic activity resulting from glass alteration. In these experiments, melt glass surface areas were increased well above the bulk glass surface areas expected for nuclear melt glass deposited in the subsurface. The debris that is incorporated into nuclear melt glass will also tend to reduce radionuclide concentrations as a result of sorption. Finally, it is expected that the maximum colloid loads achieved in these experiments are unlikely to be sustained in groundwater (e.g. (Degueldre et al., 1996a;

Degueldre et al., 1996b). Colloid filtration effects (both chemical and physical), if present, will tend to reduce ambient colloid loads which would, in turn, reduce the concentration of Pu, as well as ^{60}Co, ^{137}Cs, and ^{152}Eu. It should, therefore, not be surprising that radionuclide activities observed at ER-20-5 were approximately 1000× lower than the maximum activities observed in our melt glass alteration experiments. Similarly, the highest Pu concentration reported in contaminated NNSS groundwater from a well drilled directly into a test cavity (2.0 Bq/L, (Zhao et al., 2014)) is more than one order of magnitude lower than the maximum Pu concentrations observed in our hydrothermal nuclear melt glass alteration experiments.

The radiologic composition of these fluids before and after vacuum filtration provides information regarding radionuclide associations with colloids. Based on all the samples collected, the Pu associated with the >20 nm colloidal fraction accounts for an average of 82 % of the total Pu in solution (ranging from 68 to 94 %). The true fraction of Pu associated with colloids may be higher; Kersting et al. (1999) demonstrated that a significant fraction of colloidal Pu may fall in the 7-50 nm range. Nevertheless, our results are consistent with the field observation that the majority of Pu will be associated with colloidal materials in solution. In the case of ^{60}Co, ^{137}Cs, and ^{152}Eu, the average fraction of radionuclides associated with the >20 nm colloidal fraction is 90 %, 33 %, and 77 % compared to >90 % reported in Kersting et al. (1999) for all three radionuclides. The significantly lower ^{137}Cs association with colloids in the hydrothermal experiments compared to ER-20-5 may be indicative of the loss of aqueous ^{137}Cs as the contaminant moves down-gradient. This is also suggested by the somewhat higher ^{137}Cs/Pu ratios in our hydrothermal experiment compared to the values reported at ER-20-5 (Kersting et al., 1999).

An important observation is that, for all colloid samples, the Pu concentration associated with colloids, on a mass basis, is similar to the Pu concentration in the original melt glass. Thus, there does not appear to be a substantial partitioning of Pu into the colloidal fraction during melt glass alteration. This indicates that, to first order, the Pu concentration in the colloids will be similar to the Pu concentration in the original melt glass (i.e. ~60 ppb, on average). This observation, combined with estimates of colloid loads in groundwater, provide a means to estimate potential Pu concentrations in NNSS waters. The Pu concentration in the melt glass used in our experiments was 46.6 Bq/g. Based on the estimated stable and transient colloid concentrations that can be expected in low ionic strength deep crystalline rock groundwater ($\leq$0.0001 and $\leq$0.01 g/L, respectively), we can estimate maximum Pu concentrations that may be present in NNSS waters ($\leq$0.00466 Bg/L and $\leq$0.466 Bq/L, respectively). Interestingly, these values fall at or below the EPA MCL for Pu in drinking water. The maximum value (0.466 Bq/L) is also consistent with the highest Pu concentration measured in a post-shot hole at the NNSS (0.870 Bq/L, U-19ad PS#1A, sampled in 5/1/2008; Zhao et al., 2014). These concentrations would tend to decrease with time and migration distances due to desorption and colloid filtration processes. This suggests that Pu is unlikely to migrate downgradient from underground nuclear tests at concentrations above the EPA MCL for drinking water.

The morphology and mineralogical composition of the colloids follows that of the secondary precipitates observed as a result of melt glass alteration. The colloid characteristics were dominated by smectite minerals at both 140 and 200°C at 457 days (Figure 7). The colloid characteristics were equivalent at 994 days (not shown). While present only at trace levels, SEM and TEM revealed the presence of small iron oxide nanoparticles (Figure 8) which could be identified as magnetite and were morphologically identical to the magnetite inclusions observed

in the melt glass. Thus, it appears that the magnetite nanoparticles are released and form mobile colloids upon the dissolution of the silicate glass. While the magnetite concentrations are too low to have a substantial impact on radionuclide concentration in groundwater, they may provide a fingerprint for the presence of fluids that have contacted hydrothermally altered nuclear melt glass.

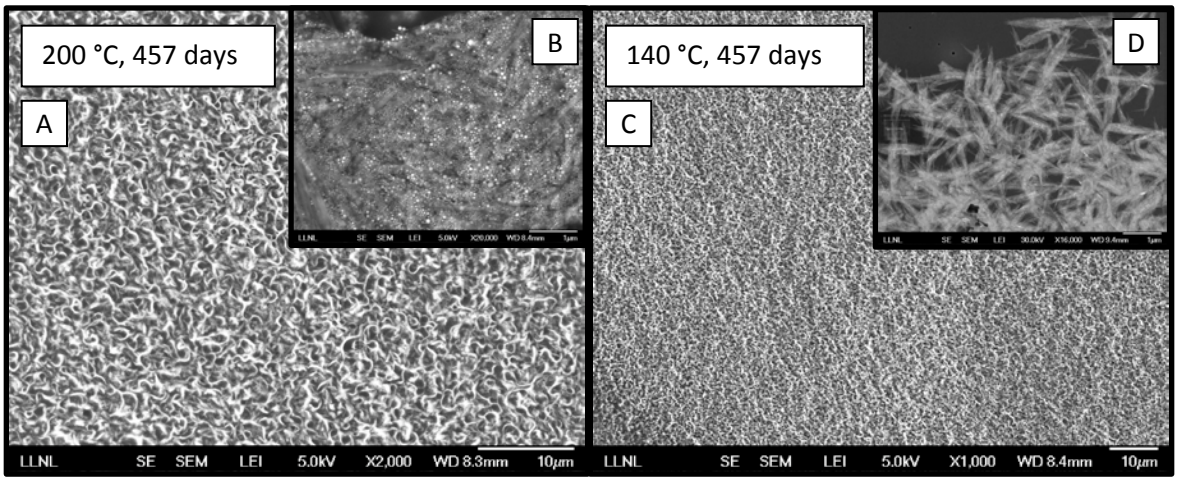

Figure 7. Colloids produced at 200°C are dominated by (A) smectite colloids. However, a trace iron oxide phase was also identified (B, small bright dots). Similar smectite colloids are produced at 140°C (C) which exhibit the layered structure of smectite colloids when viewed in transmission mode (D).

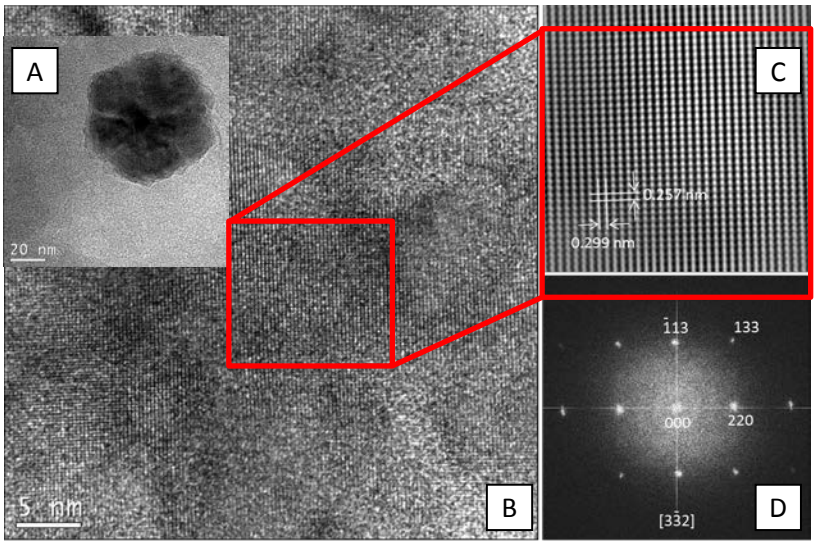

Figure 8. (A) Iron oxide nanoparticle identified as trace component in 140 °C colloidal sample, (B) HRTEM image of a Fe-rich particle identified in 140 °C colloids at 457 days, (C) enlarged HRTEM image, and (D) FFT of HRTEM image (C).

XRD data of colloidal material indicates, in agreement with SEM and TEM observations, that smectite minerals dominate at both 140 and 200°C (Figure 8). Sufficient colloidal material was not produced to allow XRD data to be collected in room temperature and 80°C colloid samples. The 200°C colloid data indicate that at 457 days, only smectite colloids were present. However, in the 644 days sample, diffraction patterns associated with the zeolite heulandite appear. The formation of zeolites at high temperature and over the long-term is consistent with observations of melt glass alteration and follows the expected formation characteristics of hydrothermally altered rhyolitic glasses.

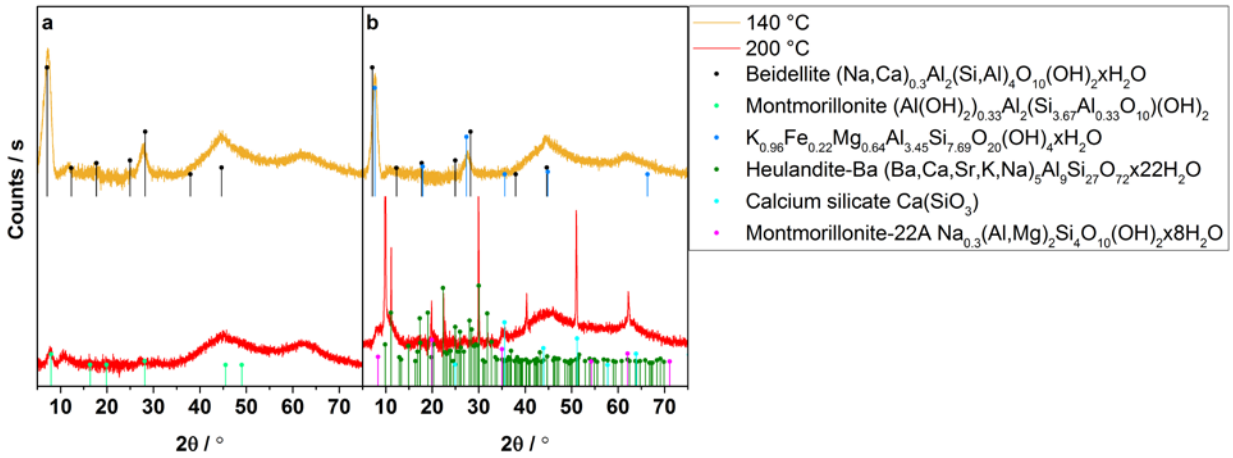

Figure 8. X-ray diffractograms of colloidal samples hydrothermally formed at 140 and 200°C after (a) 457 days and (b) 644 days.

Desorption behavior of colloids

Upon completion of the hydrothermal glass alteration experiments, subsamples of the >20 nm colloidal material were used to evaluate the Pu desorption characteristics of the hydrothermally produced colloids. Of particular interest was whether the Pu desorption behavior of these colloids follows that which we would expect from Pu adsorbed to montmorillonite which was investigated in an individual experiment (cf. Materials and Methods). In both cases, EDTA was used to desorb Pu from the mineral surfaces. EDTA is known to form relatively stable complexes with Pu in all its oxidation states (Hummel et al., 2005). However, EDTA is a strong complexing agent which also complexes ions released from the mineral itself (Fein, 2002). Consequently, it may also alter the mineral surfaces with time. Therefore, only a relatively short desorption time of four days was used in our desorption experiments.

In the case of the ^{238}Pu desorption from montmorillonite, after four days about 86% of the initial ^{238}Pu in the suspension could be desorbed from the clay surface. About 6% of ^{238}Pu was found in the original supernatant which was exchanged before the desorption experiment started. This indicates that about 8% of ^{238}Pu remains associated with the clay. An additional extraction

cycle did not significantly increase the amount of desorbed ^{238}Pu. This suggests the presence of an irreversibly sorbed Pu form. While the nature of this irreversibly sorbed Pu cannot be determined from these simple desorption experiments, we hypothesize that Pu precipitation on the clay surface, sorption in the clay interlayers, or very strong Pu surface complexes may lead to an apparently irreversible Pu sorption. Additional experiments are needed to examine the role of each of these processes.

The corresponding results for the Pu desorption from the melt glass colloidal fraction stand in clear contrast to the observations from the Pu desorption from montmorillonite. At this point of investigation it cannot be concluded whether the Pu desorption is simply kinetically limited (stronger surface complex) or truly irreversible (interlayer deposit, surface precipitation, integration in crystal structure). However, it is apparent that the fractions of reversibly- and irreversibly-sorbed Pu differ significantly between the adsorption and hydrothermal alteration experiments.

Table 3. Desorbed amount of Pu from the colloidal fraction after four days equilibration with EDTA.

Time	Desorbed Pu, %			
	25 °C	80 °C	140 °C	200 °C
457 days	NA	NA	NA	NA
644 days	NA	7	3	3
994 days	ND	11	8	6

* NA=not analyzed. ND=not detected.

While the desorption experiment was limited in scope, it suggests that desorption of Pu from clays produced as a result of hydrothermal alteration of melt glass will be less pronounced than Pu adsorbed to montmorillonite under ambient conditions. This suggests that the Pu-colloid association may not be entirely composed of a simple adsorbed species. Some fraction of the Pu may, in fact, have co-precipitated with the secondary phases as they were forming. While direct

evidence cannot be provided with these experiments given the trace Pu concentrations in these glasses, additional experiments that explore the nature of the Pu-colloid association are needed.

Acknowledgements

This work was supported by the Subsurface Biogeochemical Research Program of the U.S. Department of Energy's Office of Biological and Environmental Research and the Underground Test Area activity. Prepared by LLNL under Contract DE-AC52-07NA27344.

References

Bates, J. K., Bradley, J. P., Teetsov, A., Bradley, C. R., and Buchholtz ten Brink, M., 1992. Colloid formation during waste form reaction: Implications for nuclear waste disposal. *Science* **256**, 649-651.

Buck, E. C. and Bates, J. K., 1999. Microanalysis of colloids and suspended particle from nuclear waste glass alteration. *Applied Geochemistry* **14**, 635-653.

Carle, S. F., Maxwell, R. M., and Pawloski, G. A., 2003. Impact of Test Heat on Groundwater Flow at Pahute Mesa, Nevada Test Site. Lawrence Livermore National Laboratory, Livermore, California.

Carle, S. F., Zavarin, M., Shumaker, D. E., Tompson, A. F. B., Maxwell, R. M., and Pawloski, G. A., 2006. Simulating Effects of Non-Isothermal Flow on Reactive Transport of Radionuclies Originating from an Underground Nuclear Test*Computational Methods in Water Resources XVI*. The Technical University of Denmark, Copenhagen, Denmark.

Declercq, J., Diedrich, T., Perrot, M., Gislason, S. R., and Oelkers, E. H., 2013. Experimental determination of rhyolitic glass dissolution rates at 40-200 degrees C and 2 < pH < 10.1. *Geochimica Et Cosmochimica Acta* **100**, 251-263.

Degueldre, C., Baeyens, B., Goerlich, W., Riga, J., Verbist, J., and Stadelmann, P., 1989. Colloids in Water from a Subsurface Fracture in Granitic Rock, Grimsel Test Site, Switzerland. *Geochimica Et Cosmochimica Acta* **53**, 603-610.

Degueldre, C., Grauer, R., and Laube, A., 1996a. Colloid properties in granitic grounwater systems. II: Stability and transport study. *Applied Geochemistry* **11**, 697-710.

Degueldre, C., Pfeiffer, H. R., Alexander, W., Wernli, B., and Bruetsch, R., 1996b. Colloid properties in granitic groundwater systems. I: Sampling and characterization. *Applied Geochemistry* **11**, 677-695.

Degueldre, C., Triay, I., Kim, J., Vilks, P., Laaksoharju, M., and Miekeley, N., 2000. Groundwater colloid properties: a global approach. *Applied Geochemistry* **15**, 1043-1051.

DOE, 2000. United States Nuclear Tests: July 1945 through September 1992. Department of Energy, Las Vegas, Nevada.

Fein, J. B., 2002. The effects of ternary surface complexes on the adsorption of metal cations and organic acids onto mineral surfaces. In: Hellmann, R. and Wood, S. A. Eds.), *Water-Rock Interactions, Ore Deposits, and Environmental Geochemistry: A Tribute to David A. Crerar*. The Geochemical Society, Special Publication No. 7.

Hummel, W., Anderegg, G., Puigdomenech, I., Rao, L., and Tochiyama, O., 2005. *Chemical Thermodynamics of Compounds and Complexes of U, Np, Pu, Am, Tc, Se, Ni and Zr with Selected Organic Ligands*. Elsevier, Amsterdam.

IAEA, 1998. The Radiological Situation at the Atolls of Mururoa and Fangataufa: Main Report. International Atomic Energy Agency, Vienna.

Kersting, A. B., Efurd, D. W., Finnegan, D. L., Rokop, D. J., Smith, D. K., and Thompson, J. L., 1999. Migration of plutonium in ground water at the Nevada Test Site. *Nature* **397**, 56-59.

Kobashi, A., Choppin, G. R., and Morse, J. W., 1988. A Study of Techniques for Separating Plutonium in Different Oxidation-States. *Radiochimica Acta* **43**, 211-215.

Mazer, J. J., 1987. Kinetics of Glass Dissolution as a Function of Temperature, Glass Composition, and Solution pHs, Northwestern University.

Navarro-Intera, l., 2014. UGTA Geochemistry Database. In: Zavarin, M. (Ed.), Las Vegas, NV.

Smith, D. K., Finnegan, D. L., and Bowen, S. M., 2003. An inventory of long-lived radionuclides residual from underground nuclear testing at the Nevada test site, 1951-1992. *Journal of Environmental Radioactivity* **67**, 35-51.

Zavarin, M., Powell, B. A., Bourbin, M., Zhao, P., and Kersting, A. B., 2012. Np(V) and Pu(V) Ion Exchange and Surface-Mediated Reduction Mechanisms on Montmorillonite. *Environ. Sci. Technol.* **46**, 2692-2698.

Zhao, P., Tinnacher, R. M., Zavarin, M., and Kersting, A. B., 2014. Analysis of trace neptunium in the vicinity of underground nuclear tests at the Nevada National Security Site. *Journal of Environmental Radioactivity* **137**, 163-172.